ELSEVIER

Journal of Organometallic Chemistry 557 (1998) 121–130

Journal of Organometallic Chemistry

Organometallic compounds as single-source precursors to nanocomposite materials: an overview

Joseph P. Carpenter [a], C.M. Lukehart [a,*], Stephen B. Milne [a], S.R. Stock [b], James E. Wittig [c], Bobby D. Jones [d], Robert Glosser [d], Jane G. Zhu [e]

[a] *Department of Chemistry, Vanderbilt University, Nashville, TN 37235, USA*
[b] *School of Materials Science and Engineering, Georgia Institute of Technology, Atlanta, GA 30332, USA*
[c] *Department of Applied and Engineering Sciences, Vanderbilt University, Nashville, TN 37235, USA*
[d] *Department of Physics, University of Texas at Dallas, Richardson, TX 75083, USA*
[e] *Solid-State Division, Oak Ridge National Laboratory, Oak Ridge, TN 37831, USA*

Received 9 July 1997; received in revised form 23 July 1997

Abstract

Molecularly doped silica xerogels are prepared by adding either main-group or transition metal organometallic compounds containing bifunctional ligands to conventional sol–gel formulations. These bifunctional ligands contain distal (alkoxy or hydroxy)silyl groups, so that the dopant molecules become covalently incorporated into the silica xerogel matrix as it is being formed. Subsequent thermal treatment under reducing or oxidizing-then-reducing conditions leads to the decomposition of molecular precursor and to the formation of a nanoparticulate material with precise stoichiometry highly dispersed throughout the xerogel matrix.

Keywords: Nanocomposites; Nanoparticles; Silica xerogels; Sol–gel chemistry

1. Introduction

Nanocomposite materials consisting of particles with diameters less than 100 nm of a guest substance dispersed throughout a host matrix are a topic of intense current interest for potential applications as chemical catalysts and as photonic or magnetic materials [1]. A challenge in preparing nanocomposites is the ability to control the elemental composition and stoichiometry of the nanocluster phase.

In this overview, organometallic complexes of transition or main group metals are used as single-source molecular precursors to form nanoclusters of metal, intermetallic, metal carbide, metal phosphide or elemental germanium compositions dispersed throughout a silica xerogel matrix. These molecular precursors contain bifunctional substituents or ligands that bond covalently to core atoms within the molecular precursor and also contain a distal (alkoxy or hydroxy)silyl functional group. Addition of these molecular precursors to conventional silica sol–gel formulations gives, through hydrolysis and subsequent heterocondensation reactions, silica xerogels covalently doped with these precursor molecules. Thermal treatment of these molecularly doped xerogels under appropriate conditions affords nanocomposite products. Using this strategy, nanocomposites containing crystalline nanoclusters of Os, PtSn, Co_3C, Fe_2P, Co_2P, Ni_2P or Ge have been prepared and characterized. Control of the nanoparticulate composition through the proper choice of precursor molecule provides a 'molecules-to-nanocomposite' synthetic strategy for preparing nanocomposite materials.

* Corresponding author. Tel +1 615 3222861; fax: +1 615 3224936.

0022-328X/98/$19.00
PII S0022-328X(97)00740-7

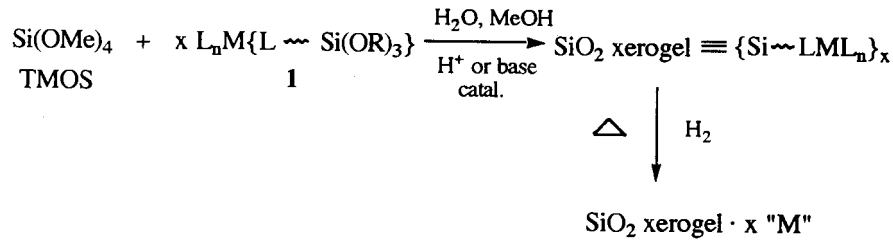

Scheme 1. Synthetic strategy for the preparation of silica xerogel nanocomposites.

2. Experimental

2.1. Synthetic methods

Although detailed procedures for syntheses discussed in this overview will be reported in more specialized journals, the experimental procedures followed in the preparation of the Co_3C/silica xerogel and Ge/silica xerogel nanocomposites are both exemplary and available [2,3]. The overall synthetic strategy is shown in Scheme 1. An organometallic complex, **1**, is prepared containing a bifunctional ligand or substituent which bears an (alkoxy or hydroxy)silyl functional group. Addition of **1** to a conventional sol–gel synthesis of silica xerogel (using tetramethylorthosilicate (TMOS), water, methanol and/or DMF or THF as cosolvents and an acid or base catalyst) gives a silica xerogel in which the dopant molecule is covalently attached to the xerogel matrix. Thermal treatment of this doped xerogel under appropriate conditions affords a silica xerogel containing a specific nanoparticulate guest substance.

Bifunctional reagents used in this study include the commercially available thiol, $HS(CH_2)_3Si(OMe)_3$ and the phosphines, $PPh_2CH_2CH_2Si(OMe)_3$ or $PPh_2CH_2CH_2Si(OEt)_3$, which were prepared according to literature procedures [4]. The molecular precursors, **1**, were prepared using published procedures or procedures reported for the preparation of analogous thiolate or phosphine complexes as indicated below.

Conventional sol–gel formulations were used in the syntheses of all molecularly doped silica xerogels [5]. Xerogels were formed at room temperature using aqueous HNO_3 or HCl as acidic catalysts or aqueous ammonia as a basic catalyst. Reaction stoichiometries for the molar ratio of total Si to molecular dopant complex are specified below but can be widely varied. Product xerogels were washed several times with alcohol prior to air or vacuum drying.

Conversion of the molecularly doped xerogels to nanocomposite materials was accomplished by placing the powdered xerogel into an alumina boat. Such samples were then introduced into a quartz tube placed inside of a tube furnace. The atmosphere within the tube was controlled by gaseous flow (150 ml min^{-1}) of the appropriate gas. Temperatures were measured using an internal thermocouple. Specific preparative and thermal conditions are described below.

2.2. Characterization methods

The nanocomposite materials were characterized using a Philips CM20T transmission electron microscope operating at 200 kV. Samples for TEM were prepared by dispersing a powdered sample of nanocomposite onto a 3-mm diameter copper grid covered with amorphous carbon as a substrate. These samples were analyzed with standard bright-field (BF) imaging for particle size distribution, selected area diffraction (SAD) for their crystal structures, and X-ray energy dispersive spectroscopy (EDS) for semi-quantitative chemical composition. Interpretation of polycrystalline SAD ring patterns was unambiguous for simple cubic crystal structures. However, for less symmetrical structures, single-crystal electron diffraction patterns were also employed to deduce the crystal structures in the nanocomposite materials.

X-ray diffraction (XRD) scans were obtained using a Philips PW1800 $\theta/2\theta$ automated powder diffractometer equipped with a Cu target and a post-sample monochromator. Samples for XRD were prepared by placing a uniform layer of powdered nanocomposite onto double-sided tape affixed to the sample holder. The sample area was greater than the ca. 1×1 cm area irradiated by the X-ray beam. Considerable caution was used to keep the top of the sample surface flat and coplanar with the diffractometer rotation axis. Prior to peak width measurement, each diffraction peak was corrected for background scattering and was stripped of the $K\alpha_2$ portion of the diffracted intensity. In suitable samples, the full width at half maximum (FWHM) was measured for each peak. Crystallite size, L, was calculated from Scherrer's equation, $L = K\lambda/\beta \cos\theta_B$, for peak broadening from size effects only (where β is the peak FWHM measured in radians on the 2θ scale, λ is the wavelength of X-rays used, θ_B is the Bragg angle for the measured *hkl* peak, and K is a constant equal to 1.00 for L taken as the volume-averaged crystallite dimension perpendicular to the *hkl* diffraction plane) [6].

3. Results and discussion

3.1. A metal/silica xerogel nanocomposite

Reaction of $[(\eta^6\text{-}p\text{-cymene})OsCl_2]_2$ with the appropriate bifunctional phosphine gives the orange mononuclear complex **2** [7]. Covalent incorporation of **2** into a silica xerogel occurs readily to give an orange xerogel (Eq. (1)). Subsequent thermal treatment under reducing conditions affords a black nanocomposite containing nanocrystals of osmium metal.

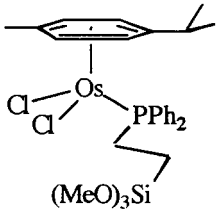

2

TMOS, H_2O/THF
H^+ catal.
Si/Os = 50/1

SiO_2 xerogel
‖
$\{[SiCH_2CH_2Ph_2P]Os(\eta^6\text{-cymene})Cl_2\}$

(1)

$\triangle$ | H_2 (900 C, 0.5 h)

SiO_2 xerogel · x Os

While reported preparations of Os nanocomposites are lacking, possibly owing to formation of the very volatile intermediate, OsO_4, Psaro and coworkers observed that $Os_3(CO)_{12}$ supported on a silica surface decomposes under hydrogen at 573 K to give Os particles [8]. By using complex **2** as a single-source precursor and a reducing thermal treatment, formation of a bulk Os/silica xerogel nanocomposite is achieved.

3.2. A binary intermetallic/silica xerogel nanocomposite

The yellow Pt–Sn heterodinuclear organometallic complex **3** is obtained by reaction of *cis*-$Pt(PPh_3)_2(Ph)(SnPh_2Cl)$ and the bifunctional thiol, $HS(CH_2)_3Si(OMe)_3$, via nucleophilic displacement of halide [9]. Covalent incorporation of **3** into a silica xerogel gives, after thermal treatment in a reducing atmosphere, a nanocomposite containing crystalline nanoclusters of the known hexagonal intermetallic compound, PtSn (niggliite), as the only observed phase (Eq. (2)). As formed, these PtSn nanoclusters have a monomodal particle size distribution with particle diameters ranging from 2 to 14 nm and an average size of 6 nm (by XRD). Prolonged thermal treatment leads to the formation of particles having an average size of 12 nm (by XRD). EDS spectra reveal the presence of Si, Pt, and Sn with no phosphorus being detected. Electron diffraction ring patterns show five rings that have *d*-spacings consistent with those known for PtSn (niggliite).

Transmission electron microscopy (TEM) images of this nanocomposite reveal nearly spheroidal osmium nanoclusters having an average diameter of 2.1 nm and a monomodal particle-size distribution with particle diameters ranging from 1 to 7 nm. An XRD scan (Fig. 1) shows one broad peak having the correct 2θ value for the *101* peak expected of crystalline osmium. The average Os particle size calculated from the width of this XRD peak using Scherrer's equation is 5.5 nm. A selected area diffraction pattern of this nanocomposite can be successfully indexed as metallic osmium. EDS spectra reveal the presence of Si and Os with no emissions for chlorine or phosphorus being detected. Thermal degradation of the molecular precursor **2** under solely reducing conditions to form Os nanoclusters is complete at least at the detection level of EDS (ca. 0.2–1.0 wt.%).

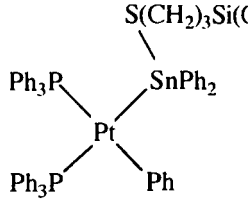

3

TMOS, H_2O/THF
H^+ catal.
Si/Pt = 30/1

SiO_2 xerogel
‖
$\{[Si(CH_2)_3SPh_2SnPt(Ph)(PPh_3)_2\}$

(2)

$\triangle$ | H_2 (700 C, 2 h)

SiO_2 xerogel · x PtSn (niggliite)

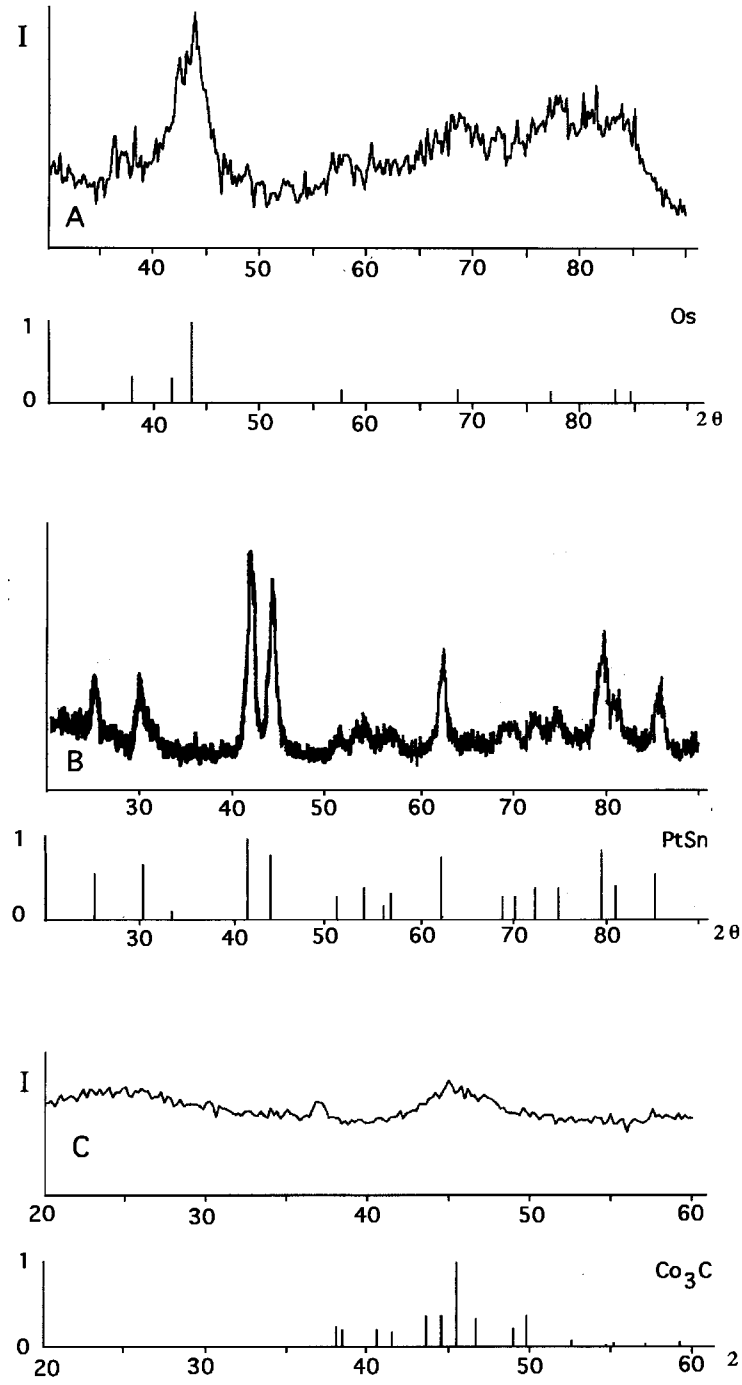

Fig. 1. XRD scans of silica xerogel nanocomposites containing nanoclusters of (A) Os, (B) PtSn or (C) Co_3C, along with XRD scans of the corresponding pure substances recorded with CuKα radiation.

Selective formation of crystalline nanoparticulate PtSn is confirmed by an XRD scan of this PtSn nanocomposite (Fig. 1). Although five different Pt/Sn compositions (Pt_3Sn, PtSn, Pt_2Sn_3, $PtSn_2$ and $PtSn_4$) are present in the Pt/Sn phase diagram, only nanoclusters of PtSn are formed from **3** [10]. Successful formation of PtSn nanoparticles from a Pt–Sn 1:1 molecular precursor demonstrates synthetic control of the elemental composition and stoichiometry of a nanocluster material through proper choice of the core structure of a molecular precursor. Nanoparticulate Pt–Sn intermetallic compounds have been studied extensively because of their importance as hydrocarbon reforming catalysts. The preparation of a single Pt–Sn composition has rarely been achieved using other synthetic methods [11].

3.3. A binary metal carbide/silica xerogel nanocomposite

Incorporation of the known purple tricobalt carbido cluster, **4**, [12] into a silica xerogel matrix gives a purple xerogel product (Eq. (3)) [2]. The intensity of the purple color deepens with increasing loading levels of complex **4**. As expected, FTIR spectra of the molecularly doped xerogel show characteristic terminal C–O stretching bands near 2065 cm^{-1}. In a control reaction, the purple methylidyne cluster, $(\mu^3\text{-HC})Co_3(CO)_9$, also appears to incorporate into the silica xerogel; however, normal washing of this purple xerogel product leads to complete extraction of the purple precursor. These observations are consistent with the covalent incorporation of **4** in the xerogel matrix. Hydrolysis products from the TMOS sol–gel conversion presumably undergo heterocondensation with the trihydroxysilyl substituent of complex **4** [2].

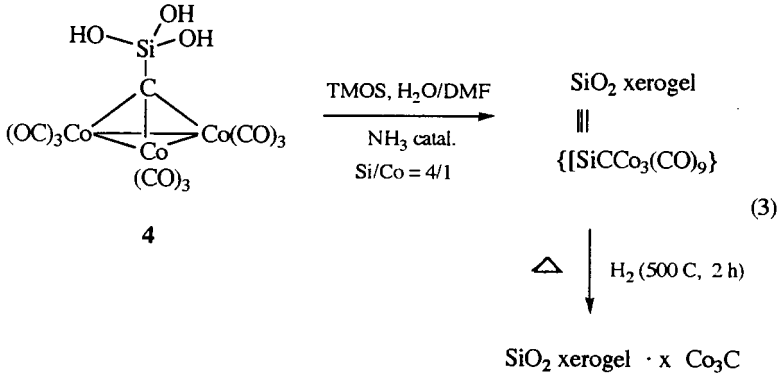

When the purple silica xerogel doped with **4** is heated in a hydrogen atmosphere, a black xerogel powder is obtained. Upon exposure to air, the black powder slowly turns gray indicating possible air oxidation of a component phase. An FTIR spectrum of this black product reveals the expected absence of carbonyl ligand C–O stretching bands. TEM micrographs reveal nearly spheroidal particles of a guest phase dispersed throughout the xerogel. A monomodal particle-size distribution is observed with particle diameters ranging from 10 to 46 nm and an average particle diameter of 25 nm. An EDS scan reveals X-ray emissions confirming the presence of silicon and cobalt. EDS scans of selected on-particle and off-particle areas confirms the concentration of cobalt within the particulate features.

Electron diffraction from this nanocomposite gives a complex SAD ring pattern consistent with the known diffraction pattern for orthorhombic Co_3C. Interplanar spacings calculated from a single-crystal spot pattern are also consistent with the known unit cell of Co_3C crystal. These electron diffraction data strongly support the presence of Co_3C as the principal crystalline material within the nanocomposite.

An XRD scan of the Co_3C/silica xerogel nanocomposite along with the standard XRD scan of orthorhombic Co_3C are shown in Fig. 1. A broad peak centered at ca. 25° in 2θ arises from amorphous scattering from the silica xerogel host matrix. The most intense peak centered at ca. 45° in 2θ is assigned to several overlapping peaks expected for crystalline Co_3C. The presence of crystalline Co_3O_4 is indicated by the relatively weak peak centered at ca. 37° in 2θ. The low overall intensity of XRD peaks assigned to crystalline Co_3C results from the relatively low doping level of this material and from the low symmetry of this crystalline lattice. The presence of cobalt metal or other cobalt carbide structures is not observed. The origin of the Co_3O_4 material is unknown, although oxidation of cobalt could occur during the sol–gel synthesis of the nanocomposite material or during its subsequent handling prior to analysis by TEM or XRD.

The formation of Co_3C nanoclusters is particularly noteworthy given that several cobalt carbide phases are known. Furthermore, the elemental composition of this cobalt carbide phase is precisely that of the core structure of complex **4**, thereby providing another example of synthetic control of nanocluster composition through proper choice of molecular precursor.

3.4. Binary metal phosphide/silica xerogel nanocomposites

Transition metal phosphine complexes can serve as single-source molecular precursors to metal phosphide/silica xerogel nanocomposites as shown in Eqs. (4)–(6). The molecular precursors, $Fe(CO)_4[PPh_2CH_2CH_2Si(OMe)_3]$, **5**, $Co_2(CO)_6[PPh_2CH_2CH_2Si(OEt)_3]_2$, **6**, and $Ni[PPh_2CH_2CH_2Si(OEt)_3]_4$, **7**, are synthesized using published procedures or those reported for the preparation of analogous complexes [13–17], and the presence of bifunctional phosphine ligands leads to the direct covalent incorporation of these complexes into a silica xerogel matrix. Conversion of these

molecularly doped xerogels to nanocomposites is accomplished by thermal treatment under the reducing conditions shown.

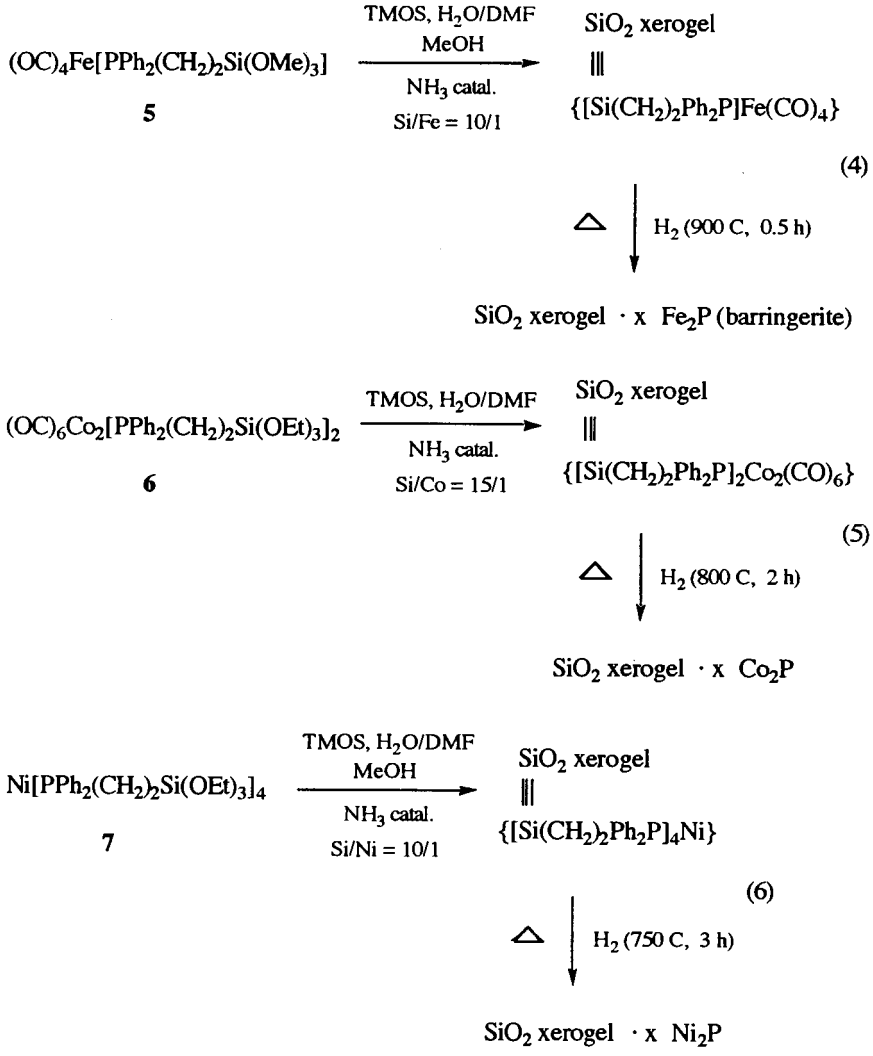

TEM micrographs of these metal phosphide/silica xerogel nanocomposites reveal nearly spheroidal particles for the Co_2P and Ni_2P nanoclusters. However, the Fe_2P (hexagonal barringerite) nanoclusters show sharp edges and corners with some particles oriented properly to give a hexagonal projection (Fig. 2). Fe_2P particle diameters range in value from 2 to 8 nm with an average value of 4.7 nm.

On-particle EDS spectra indicate a Fe:P ratio of 1.98:1 which is consistent with the formula, Fe_2P. Selected area diffraction ring patterns obtained from this nanocomposite reveal seven rings having *d*-spacings which match well with those reported for Fe_2P. A spot pattern obtained by electron diffraction from one nanocrystal of Fe_2P can be indexed using the cell parameters of barringerite. An XRD scan of this nanocomposite shows peaks that match well in 2θ values and in relative intensities with the corresponding *111*, *201*, and *210* XRD peaks of barringerite (Fig. 3). Measurement of the full width at half maximum of each of these three peaks and application of Scherrer's equation gives a volume-averaged mean particle diameter of 10 nm. This nanocomposite apparently contains a small fraction of Fe_2P particles having diameters significantly larger than 4.7 nm.

Co_2P nanoclusters have particle diameters ranging in value from 2.5 to 10 nm with an average particle diameter of 5 nm. EDS spectra indicate the presence of both Co and P, and *d*-spacings derived from the observed selected area electron diffraction ring patterns (six rings) for this nanocomposite are consistent with the known orthorhombic Co_2P crystalline phase. On-particle EDS spectra indicate a Co:P ratio of 2.09:1 which is consistent with the formula, Co_2P. An XRD scan of this nanocomposite confirms the presence of crystalline Co_2P with no other crystalline phases being evident (Fig. 3).

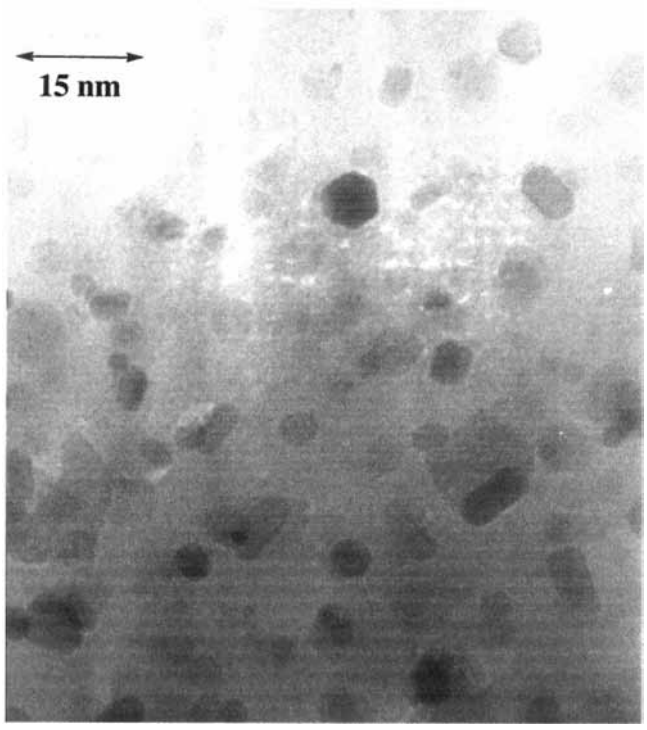

Fig. 2. TEM image of a silica xerogel nanocomposite containing hexagonal nanocrystals of Fe_2P (barringerite).

Ni_2P particle diameters range in value from 0.7 to 3.7 nm with an average particle diameter of 2.6 nm. EDS spectra obtained from the Ni_2P nanocomposite confirm the presence of both Ni and P in this product xerogel. Selected area diffraction ring patterns obtained from this nanocomposite reveal five rings have *d*-spacings which match well with those reported for standard samples of hexagonal Ni_2P. An XRD scan shows peaks that match well in 2θ values and in relative intensities with the corresponding *111*, *201*, and *120* XRD peaks of Ni_2P (Fig. 3). Measurement of the full width at half maximum of each of these three peaks and application of Scherrer's equation gives a volume-averaged mean particle diameter of ca. 9 nm. This nanocomposite apparently contains a small fraction of Ni_2P particles having diameters significantly larger than 2.6 nm.

Complexes **5**–**7** clearly act as single-source molecular precursors for the formation of silica xerogel composites containing crystalline nanoparticles of the known metal phosphides, Fe_2P, Co_2P or Ni_2P, respectively. In contrast to the syntheses described in Eqs. (1)–(3), the M:P core stoichiometries of these molecular precursors do not control the M:P stoichiometry of the resulting nanoparticulate material. However, in each case selective formation of only one crystalline metal phosphide composition is observed. As listed in Table 1, seven different crystalline forms or stoichiometric compositions are known for iron phosphides. In addition, five different cobalt phosphide compositions and

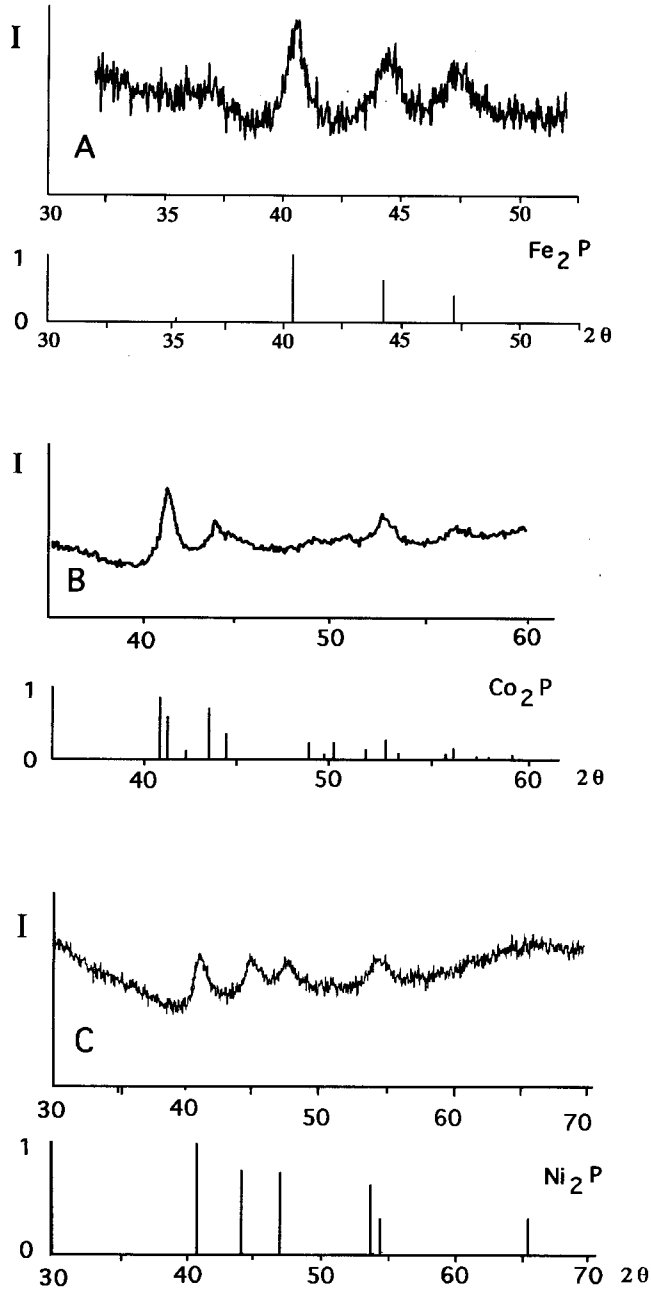

Fig. 3. XRD scans of silica xerogel nanocomposites containing nanoclusters of (A) Fe_2P, (B) Co_2P or (C) Ni_2P, along with XRD scans of the corresponding pure substances recorded with CuKα radiation.

ten different nickel phosphide compositions are also known. Under the thermal conditions employed, a unique metal phosphide composition is formed for each metal. This composition is the congruently melting phase having the highest phosphorus/metal ratio. We speculate that a type of hydrodephosphination reaction occurs during thermal treatment to remove phosphorus from the incipient metal core composition until the M:P composition of the observed congruently melting phase is reached. Further study is required to further substantiate the generality of this trend.

3.5. A germanium/silica xerogel nanocomposite

Reaction of Me_3GeBr and the bifunctional thiol, $HS(CH_2)_2Si(OMe)_3$, in the presence of triethylamine gives excellent yields of the organogermanium compound **9** [3]. Incorporation of **9** into a silica xerogel occurs readily, and thermal treatment under successive oxidizing and reducing conditions gives a silica xerogel containing crystalline nanoclusters of Ge (Eq. (7)) [3].

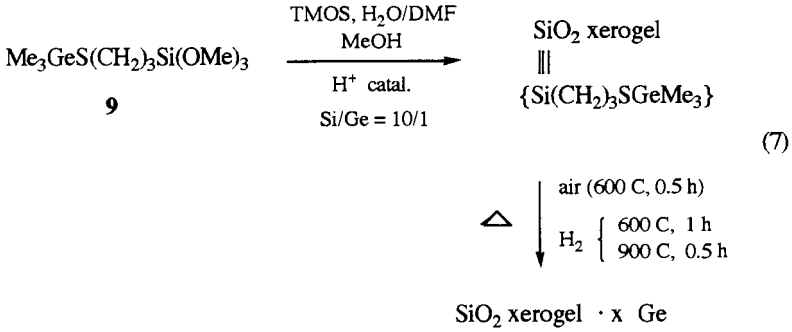

(7)

TEM micrographs reveal the presence of highly crystalline spheroidal Ge nanoclusters having diameters in the range 2.5–14.5 nm with an average diameter of 6.7 nm. The high crystallinity of the Ge particulates is evident in the HRTEM image shown in Fig. 4. Two sets of *111* lattice fringes are observed extending across the entire diameter of the nanocluster. The background of the micrograph depicts the amorphous silica xerogel matrix.

Electron diffraction SAD patterns obtained from this nanocomposite reveal three prominent rings assignable to the *111*, *220*, and *311* planes of crystalline germanium. SAD patterns obtained from nanocomposites prepared from more heavily doped xerogels reveal up to six rings consistent with crystalline Ge.

An X-ray diffraction (XRD) scan of this Ge/silica xerogel nanocomposite is shown in Fig. 5. The broad peak centered near 22° in 2θ is assigned to amorphous scattering from the silica xerogel matrix. Three peaks matching the 2θ values and relative intensities of those expected for the *111*, *220* and *311* planes of crystalline Ge are the only other peaks observed. Crystallite sizes calculated from Scherrer's equation using the widths of these peaks give an average Ge nanocrystallite size of 6.8 nm. The close agreement in average particle size determined by TEM and XRD indicates that very few crystalline Ge nanoclusters have diameters significantly larger than 145 Å.

A micro-Raman spectrum of this nanocomposite is shown in Fig. 6. The sharp signal observed at 301 cm^{-1} corresponds to the phonon frequency of microcrystalline Ge. The width of this peak is consistent with Ge microcrystals having diameters of ca. 6.0 nm [18], and a

Table 1
Known compositions and unit cell symmetries for iron-, cobalt-, or nickel phosphides

Iron Phosphides	Cobalt Phosphides	Nickel Phosphides
Fe_3P, tetragonal	Co_2P, orthorhombic	Ni_3P, tetragonal
Fe_2P, hexagonal	CoP, orthorhombic	$Ni_{2.55}P$, hexagonal
FeP, orthorhombic	CoP_2, monoclinic	Ni_5P_2, hexagonal
FeP_2, orthorhombic	CoP_3, cubic	$Ni_{12}P_5$, tetragonal
FeP_4, monoclinic	CoP_4, cubic	Ni_7P_3, cubic
FeP_4, orthorhombic		Ni_2P, hexagonal
γ-FeP_4, monoclinic		Ni_5P_4, hexagonal
		NiP, orthorhombic
		NiP_2, monoclinic/cubic
		NiP_3, cubic

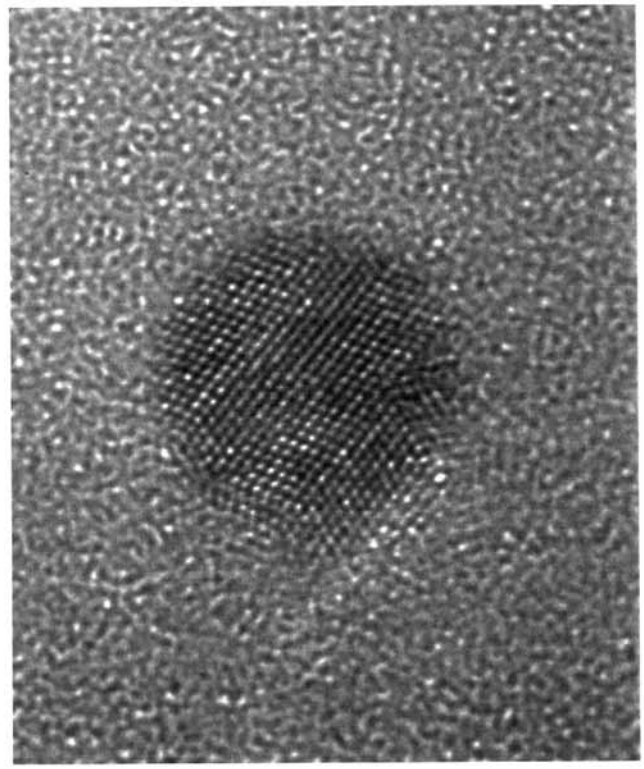

Fig. 4. High-resolution TEM image of a Ge nanocrystal in a Ge/silica xerogel nanocomposite.

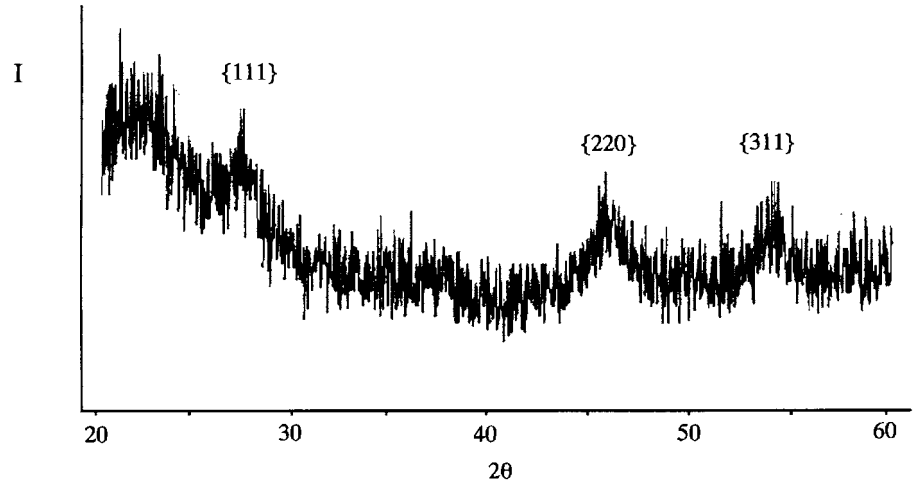

Fig. 5. XRD scan of a silica xerogel nanocomposite containing nanoclusters of Ge recorded with CuKα radiation.

small amount of non-crystalline Ge is evident by the slight trailing of the Ge phonon band to lower frequency.

4. Conclusions

Organometallic complexes can be used as single-source precursors for the preparation of a variety of bulk silica xerogel nanocomposites. Osmium nanoclusters are formed directly from thermal degradation of a low-valent precursor under reducing conditions, thus obviating the need for oxidative degradation of the precursor affording volatile metal-oxide intermediates. Crystalline nanoparticulates of the binary substances PtSn and Co_3C can be prepared with stoichiometric precision using molecular precursors having molecular cores of these exact compositions. Nanoparticulate metal phosphide substances are formed as single phases from metal phosphine molecular precursors by loss of phosphorus from the incipient molecular cores. An organogermanium compound serves as a single-source precursor to crystalline germanium nanoclusters. The successful preparation of these silica xerogel nanocomposites represents another application of organometallic chemistry to materials science and a beginning in the development of new synthetic strategies for controlling the chemical composition of nanoparticulate materials.

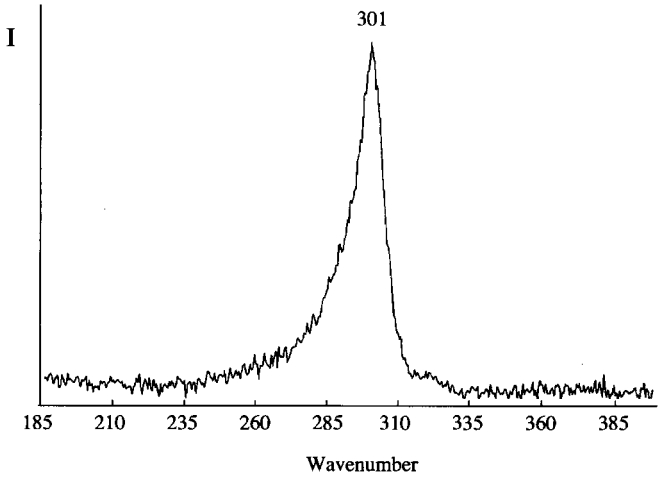

Fig. 6. Micro-Raman spectrum of a Ge/silica xerogel nanocomposite showing the phonon band of the Ge nanoclusters.

Acknowledgements

This material is based upon work supported by, or in part by, the U.S. Army Research Office under grant number DAAH04-95-1-0146. C.M.L. is grateful for this support. Work performed at ORNL (J.G.Z.) was supported by DOE under Contract DE-AC05-840R21400 with Lockheed Martin Energy Systems, Inc.

References

[1] (a) G.D. Stucky, Naval Res. Rev. 43 (1991) 28. (b) G. Schmid, Chem. Rev. 92 (1992) 1709. (c) J.H. Sinfelt, G.D. Meitzner, Acc. Chem. Res. 26 (1993) 1. (d) J. Fendler, Chem. Rev. 87 (1987) 877. (e) M.L. Steigerwald, L.E. Brus, Acc. Chem. Res. 23 (1990) 183. (f) Y. Wang, Acc. Chem. Res. 24 (1991) 133. (g) J.P. Bonnelle, B. Delmon, E. Derouane, in D. Reidel (Ed.), Surface properties and catalysis by non-metals, Dordrecht, Holland, 1983. (h) S.R. Marder, J.E. Sohn, G.D. Stucky, Materials for nonlinear optics, American Chemical Society, Washington, D.C., 1991. (i) D.F. Eaton, Science 253 (1991) 281. (j) A. Henglein, Top. Curr. Chem. 113 (1988) 156. (k) H.M. Gibbs, G. Khitrova, N. Peyghanbarian (Eds.), Nonlinear photonics, Springer-Verlag, Berlin, 1990. (l) G. Schmid, Chem. Rev. 92 (1992) 1709. (m) Z. Duan, M.J. Hampden-Smith, A. Datye, J. Catal. 139 (1993) 504. (n) L.N. Lewis, Chem. Rev. 93 (1993) 2693. (o) H. Weller, Angew. Chem. Int. Ed. Engl. 32 (1993) 41. (p) H. Weller, Adv. Mater. 5 (1993) 88. (q) Y. Wang, N. Herron, W. Mahler, A.J. Suna, Opt. Soc. Am. B. 6 (1989) 808. (r) Y. Wang, W. Mahler,

Opt. Comm. 61 (1987) 233. (s) E. Hilinski, P. Lucas, Y. Wang, J. Chem. Phys. 89 (1988) 3435. (t) Y. Wang, A. Suna, J. McHugh, E. Hililnski, P. Lucas, R.D. Johnson, J. Chem. Phys. 92 (1990) 6927.
[2] J.P. Carpenter, C.M. Lukehart, S.R. Stock, J.E. Wittig, Chem. Mater. 7 (1995) 2011.
[3] J.P. Carpenter, C.M. Lukehart, D.O. Henderson, R. Mu, B.D. Jones, R. Glosser, S.R. Stock, J.E. Wittig, J.G. Zhu, Chem. Mater. 8 (1996) 1268.
[4] H. Niebergall, Makromol. Chem. 59 (1962) 218.
[5] (a) T. Adachi, S. Sakka, J. Mater. Sci. 22 (1987) 4407. (b) C.J. Brinker, G.W. Scherer, Sol–gel science, Academic Press, New York, 1990.
[6] H.P. Klug, L.E. Alexander, X-ray diffraction procedures for polycrystalline and amorphous materials, second edition, Wiley and Sons, New York, 1974.
[7] J.A. Cabeza, P.M. Maitlis, J. Chem. Soc., Dalton Trans. (1985) 573.
[8] R. Psaro, C. Dossi, A. Fisco, R. Ugo, Res. Chem. Intermed. 15 (1991) 31.
[9] C. Eaborn, A. Pidcock, B.R. Steele, J. Chem. Soc., Dalton Trans. (1976) 767.
[10] T.B. Massalski, Binary alloy phase diagrams, second edition, ASM International, Materials Park, Ohio, 1990.
[11] (a) C. Xu, J.W. Peck, B.E. Koel, J. Am. Chem. Soc. 115 (1993) 751. (b) R. Srinivasan, L.A. Rice, B.H. Davis, J. Catal. 129 (1991) 257.
[12] D. Seyferth, C.N. Rudie, M.O. Nestle, J. Organomet. Chem. 178 (1979) 227.
[13] M.J. Therien, W.C. Trogler, Inorg. Synth. 28 (1990) 173.
[14] C.S. Cundy, J. Organomet. Chem. 69 (1974) 305.
[15] L. Bemi, H.C. Clark, J.A. Davis, C.A. Fyfe, R.E. Wasylishen, J. Am. Chem. Soc. 104 (1982) 438.
[16] U. Schubert, K. Rose, H. Schmidt, J. Non-Cryst. Solids 105 (1988) 165.
[17] H. Neibergall, Makromol. Chem. 59 (1962) 218.
[18] M. Jujii, S. Hayashi, K. Yamamoto, Jpn. J. Appl. Phys. 30 (1991) 687.